

# Photocatalytic H<sub>2</sub> production from ethanol aqueous solution using TiO<sub>2</sub> with tungsten carbide nanoparticles as co-catalyst

A. Pajares<sup>1,2</sup>, M. J. Kronenberg<sup>1</sup>, P. Ramírez de la Piscina<sup>1</sup>, N. Homs<sup>1,2\*</sup>

<sup>1</sup> *Departament de Química Inorgànica i Orgànica, secció de Química Inorgànica & Institut de Nanociència i Nanotecnologia (IN2UB), Universitat de Barcelona, Martí i Franquès 1, 08028 Barcelona, Spain.*

<sup>2</sup> *Catalonia Institute for Energy Research (IREC), Jardins de les Dones de Negre 1, 08930 Barcelona, Spain.*

(\*) Corresponding author:

Narcis Homs, [narcis.homs@qi.ub.edu](mailto:narcis.homs@qi.ub.edu)

## **Abstract**

The effect of tungsten carbide as co-catalyst in the photocatalytic H<sub>2</sub> production from ethanol aqueous solutions (25% v/v) is reported. The photocatalytic H<sub>2</sub> production using WC/TiO<sub>2</sub> (1% wt WC), in which tungsten carbide NPs are dispersed onto TiO<sub>2</sub>, is compared with that of TiO<sub>2</sub>800 with morphological and structural characteristics similar to WC/TiO<sub>2</sub> and with the hydrogen produced using commercial TiO<sub>2</sub> P25 as reference. The preparation of WC/TiO<sub>2</sub> was accomplished by using a sol-gel based method which was useful for preparing bulk tungsten carbides. Materials were characterized using N<sub>2</sub> physisorption, XRD, SEM-EDX, TEM, UV-vis RDS, XP and Raman spectroscopy. The presence of 2-3 nm NPs with different tungsten carbide crystalline phases (hexagonal WC and W<sub>2</sub>C and cubic WC<sub>1-x</sub>) onto TiO<sub>2</sub>, containing anatase and rutile, was determined.

The presence of tungsten carbide NPs onto TiO<sub>2</sub> improves the photocatalytic behavior of TiO<sub>2</sub> in terms of hydrogen production. The effect of WC<sub>x</sub> NPs in the C<sub>2</sub>-C<sub>4</sub> products derived from ethanol is discussed and the reusability of the photocatalyst is also studied.

**Keywords:** *photocatalytic H<sub>2</sub>; WC co-catalyst; WC/TiO<sub>2</sub> photocatalyst; H<sub>2</sub> photoproduction; ethanol photooxidation.*

## Introduction

Hydrogen is an ideal carbon-free energy carrier, which production from renewable feedstocks merits to be implemented. Biomass-derived alcohols can be considered an efficient mean to store hydrogen in a form that is easy to handle and transport. Thus, bio-alcohols have been largely investigated as alternative renewable feedstock for H<sub>2</sub> production using catalytic reforming technology [1-3]. Nowadays, ethanol is the biofuel worldwide produced in the greatest amount; most of ethanol is produced from crops, mainly corn and sugarcane. However, new policy and programs in different countries are promoting the construction of new plants, using urban solid residues or lignocellulosic materials for bio-ethanol production, bringing the possibility of a more sustainable approach than the traditional processes [4].

From an environmental point of view, the photocatalytic transformation of bioethanol aqueous solutions could be a suitable method for H<sub>2</sub> production [5-8]. The appropriate photo-irradiation of a semiconductor-based photocatalyst promotes an electron from the valence band to the conduction band of the semiconductor. The photo-generated charges, hole (h<sup>+</sup>) and electron (e<sup>-</sup>), can move to the surface [9], then, adsorbed organic species could be oxidized by the h<sup>+</sup> or hole-related species [6,10-12], meanwhile H<sub>2</sub> is formed from H<sup>+</sup> reduction in the media [6, 13]. The ethanol oxidation process takes place in different steps and could be adjusted avoiding the CO<sub>2</sub> formation. Thus, besides H<sub>2</sub>, other C<sub>2</sub>-C<sub>4</sub> valuable products such as acetaldehyde, 2,3-butanediol or acetone can be rendered [10, 11].

The photocatalytic transformation of ethanol<sub>(aq)</sub> has been studied mainly using a semiconductor, with a noble metal as co-catalyst, Pt/TiO<sub>2</sub> being one of the most

studied systems. Pt nanoparticles (NPs) favor the electron transport, being sinks of electrons and contributing to the charge separation throughout the interface. Different approaches for the metallic phase or TiO<sub>2</sub> modification in order to improve the photocatalytic behavior have been reported [14-16]. However, the price and scarcity of noble metals have led to proposing alternative catalytic materials in different reactions in which noble metal-based catalysts are usually used. Several transition metal carbides (TMCs) exhibit metallic characteristics and since pioneering work on WC, showing its platinum-like catalytic properties [17], many studies have been carried using TMCs as catalysts in different processes [18-20]. Specifically, WC has electronic properties and density of states close to those of Pt [21, 22] and it has been largely studied in new electrocatalytic systems [23-28]. WC has been also proposed for replacing Pt in different photocatalytic reactions such as water splitting and photocatalytic degradation of organics [29-32]. A limited number of papers deals with the use of WC as co-catalyst for the photocatalytic H<sub>2</sub> generation from H<sub>2</sub>O; the role of WC onto CdS and g-C<sub>3</sub>N<sub>4</sub> has been studied using h<sup>+</sup> scavengers such as lactic acid, Na<sub>2</sub>S/Na<sub>2</sub>SO<sub>3</sub> or TEOA [32-35]. However, the use of those sacrificial agents can lead to byproducts, which are not usually studied. An early paper has reported the activity of a commercial TiO<sub>2</sub> (anatase) powder grinded with WC for the photocatalytic hydrogen production using an aqueous methanol solution [36].

In the present study, ethanol is used as h<sup>+</sup> scavenger because as stated above, it is derived from biomass and has a renewable character. Moreover, selective ethanol photo-transformation, can result in forming C<sub>2</sub>-C<sub>4</sub> valuable products such as acetaldehyde, 2,3-butanediol or acetone. Here, the use of tungsten carbide NPs as co-catalyst onto TiO<sub>2</sub> in the photocatalytic H<sub>2</sub> evolution using 25% v/v

aqueous solutions of ethanol is studied. For a better understanding of the overall photocatalytic process, the products coming from the ethanol oxidation were also determined and the O<sub>2</sub> evolution analyzed. For this end, a photocatalyst composed of WC NPs onto TiO<sub>2</sub> was prepared, characterized and tested in the photocatalytic reaction. The photocatalytic behavior of WC/TiO<sub>2</sub> is compared to that of WC-free TiO<sub>2</sub>. The amount of H<sub>2</sub> produced using WC/TiO<sub>2</sub>, is higher than that yielded using WC-free TiO<sub>2</sub>. This accords with the role of WC as co-catalyst in the photocatalytic H<sub>2</sub> generation onto TiO<sub>2</sub>. The preparation of WC/TiO<sub>2</sub>, was based on a method useful for preparing bulk WC, this method allowed obtaining well dispersed nanoparticles of WC<sub>x</sub> on TiO<sub>2</sub>.

## **Materials and Methods**

### *Catalyst preparation and characterization*

For the preparation of WC, a sol-gel method based on urea glass route was used [37]. Specifically, a 5% wt/v tungsten (IV) isopropoxide solution (20 mL) and 2.29 g of urea were added to 42 mL of ethanol. After total dissolution, the system was stirred under Ar flow for 4 h and then, the solvent was evaporated in an oven at 343 K for 16 h. After that, the solid was placed in a quartz tube and heated (2 K/min) under Ar flow up to 1073 K for 3 hours. Finally, the solid was cooled down to room temperature under Ar flow and the lustrous black powder material was transferred without passivation and stored.

The 1% wt WC/TiO<sub>2</sub> photocatalyst was obtained following a similar procedure but in the presence of commercial TiO<sub>2</sub> (Tecnan, S<sub>BET</sub>= 117 m<sup>2</sup>g<sup>-1</sup>, anatase/rutile= 78/22% wt/wt). 1.2 mL of 5% wt/v tungsten (IV) isopropoxide in isopropanol were mixed with 4.5 mL of ethanol and 0.14 g of urea under Ar flow. After dissolution,

a suspension of 2.0 g of TiO<sub>2</sub> in 25 mL of ethanol was added. The mixture was maintained with continuous stirring for 4 h, placed in an oven at 343 K for 16 hours and finally, treated up to 1073 K using the experimental procedure described above for the bulk WC preparation. A dull greyish solid was obtained in this case. For comparative purposes, the commercial TiO<sub>2</sub> used in the preparation of WC/TiO<sub>2</sub> was treated at 1073 K under Ar flow for 4 h, this sample labelled TiO<sub>2</sub>800 was characterized and tested. Moreover, the photocatalytic hydrogen production was determined using commercial TiO<sub>2</sub> P25, which is usually used as a standard material in photocatalytic studies [38].

The Brunauer-Emmett-Teller specific surface area ( $S_{\text{BET}}$ ) of the samples was calculated from the nitrogen adsorption-desorption isotherms, the Barret-Joyner-Halender (BJH) method was used for determining the pore size distribution; experiments were carried out using a Micromeritics TriStar II 3020 apparatus. The X-ray diffraction (XRD) patterns were acquired from 20 to 100° with a step of 0.017° using a PAMalytical X'Pert PRO MPD Alpha 1 powder diffractometer; Cu K $\alpha$ 1 radiation ( $\lambda = 1.5406 \text{ \AA}$ ) was employed. The crystallite sizes of anatase and rutile were calculated using the Scherrer equation. The weight percentage of rutile in the samples was determined from (110) R and (101) A diffraction peaks [39].

The morphology of the samples was analysed using a field emission scanning electron microscope (FESEM), JEOL J-7100F, operating at 20 kV. The FESEM was coupled with an X-ray analysis system (Oxford Instruments) which allowed acquire energy-dispersive X-ray (EDX) spectra and elemental mapping.

A JEOL JEM-2010 SON transmission electron microscope (TEM) operating at 200 kV was used for obtaining TEM and high resolution TEM (HRTEM) images.

For the study, ethanol dispersions of samples on copper grids were used.

The Raman spectra were obtained using a Jobin-Yvon LabRaman HR 800 instrument with a CCD detector and a 532 nm laser at 1.5 mW.

UV-vis diffuse reflectance spectra were acquire using a Perkin Elmer Lambda 950 spectrometer. The Kubelka-Munk formalism was applied, and the band-gap values were calculated through the Tauc plot  $(F(R_{\infty}) \cdot h\nu)^n$  versus  $h\nu$ , assuming an indirect allowed transition,  $n=1/2$  [40].

The characterization by X-ray photoelectron spectroscopy (XPS) was performed using a Perkin Elmer PHI-5500 Multitechnique System with a hemispherical electron energy analyser and a 1486.6 eV Al  $K\alpha$  radiation. The adventitious C 1s peak at 284.8 eV was taken as reference of binding energy values. Deconvolution of XPS peaks were done using the CasaXPS software keeping symmetric Gaussian (70%)-Lorentzian (30%) functions.

### *Photocatalytic tests*

The setup used in the photocatalytic tests, including the analysis system has been described elsewhere [10, 11]. In brief, the tests were carried out at atmospheric pressure in a jacketed reactor of 300 mL capacity designed for continuous gas flow operation and equipped with a condenser (kept at 258 K) at the outlet. A UV-visible 175 W Hg lamp (broad-spectrum lamp, maximum power of 25.6 W at  $\lambda = 366$  nm), placed inside the reactor in a water-cooled jacket was used. Before the photocatalytic reaction, the catalysts were degassed under vacuum at 373 K for 12 h, and then transferred directly to the photoreactor. 500

mg of catalyst and 250 mL of an ethanol<sub>(aq)</sub> (25% v/v) solution previously purged with Ar, were used. Before irradiation, the suspension was stirred for 30 min under Ar flow, then the system was irradiated and kept at 298 K. The gases evolving from the reactor were analyzed in dark conditions before starting and at the end of the photocatalytic test; H<sub>2</sub> was not produced in any case in dark conditions. After 10 min of light on, the evolved gaseous products were periodically sampled and on-line analyzed. The gaseous products were analyzed on-line using a gas micro-chromatograph Varian CP-4900 equipped with micro-TCD detectors and two columns. The CO<sub>2</sub> and hydrocarbon analysis was carried out using a PPQ (10 m) column and He as carrier gas. For H<sub>2</sub>, O<sub>2</sub>, N<sub>2</sub> and CO analysis (detection limit for H<sub>2</sub>, 50 ppm), a molecular sieve (5Å, 10 m) column and Ar carrier gas were used. The liquid products were separately analyzed by gas chromatography at the end of the photocatalytic test (4 h) in a Bruker 450 GC equipment with FID detector and a CP-Sil 8 CB (30 m x 0.25 mm) capillary column.

The reusability of WC/TiO<sub>2</sub> was studied after separation of the used catalyst by filtration. New photocatalytic tests were carried out with 170 mg of the used and fresh catalysts.

## **Results and discussion**

As stated in the introduction and experimental sections, bulk WC was prepared using a sol-gel based method with urea. This method was also used in the presence of commercial TiO<sub>2</sub> for the preparation of WC/TiO<sub>2</sub>, in which the co-catalyst WC is incorporated onto TiO<sub>2</sub>. For comparative purposes, a sample of commercial TiO<sub>2</sub> was treated at 1073 K (TiO<sub>2</sub>800) which is the temperature used



in the preparation of WC/TiO<sub>2</sub>. Table 1 shows some characteristics of the materials prepared. BET surface area of WC/TiO<sub>2</sub> (11 m<sup>2</sup>g<sup>-1</sup>) was only slightly lower than that of TiO<sub>2</sub>800 (15 m<sup>2</sup>g<sup>-1</sup>). Both, WC/TiO<sub>2</sub> and TiO<sub>2</sub>800 were mesoporous materials with mean pore width of 24 and 32 nm, respectively.

Figure 1 shows the XRD patterns of WC, WC/TiO<sub>2</sub> and TiO<sub>2</sub>800. For WC, the presence of tungsten carbides with poor crystallinity can be inferred; the presence of hexagonal WC (JCPDS 00-051-0939) and W<sub>2</sub>C (JCPDS 00-035-0776) and cubic WC<sub>1-x</sub> (JCPDS 00-020-1316) can be reasonably proposed. XRD patterns of WC/TiO<sub>2</sub> and TiO<sub>2</sub>800 were very similar, only peaks characteristics of anatase (A) (JCPDS 00-021-1272) and rutile (R) TiO<sub>2</sub> (JCPDS 01-076-0317) were present. In both cases, the A/R ratio was 8/92% wt/wt; the crystallite size of A and R in WC/TiO<sub>2</sub> and TiO<sub>2</sub>800, was 99, 60 (A) and 60, 59 (R) nm, respectively (Table 1). The absence of peaks characteristics of crystalline carbide phases in the XRD pattern of WC/TiO<sub>2</sub> could be probably due to the low amount of tungsten carbide in the material. Figure 2 shows a SEM image of WC/TiO<sub>2</sub> and the corresponding EDX mapping, which showed, as expected, the presence of Ti, O, W and C in the sample. EDX analysis of different zones pointed to a W content of about 1% wt. In order to confirm the presence of crystalline WC in WC/TiO<sub>2</sub>, this sample was analyzed by TEM. TEM images of WC/TiO<sub>2</sub> (Figure 3A and 3B) show particles with a mean size of 2.3 nm (inset in Figure 3C) well dispersed onto TiO<sub>2</sub>. HRTEM analysis of different tungsten carbide particles allowed to identify different planes of the W<sub>2</sub>C, WC and WC<sub>1-x</sub> phases (Figure 3C and 3D). Although the presence of crystalline tungsten oxides in WC and WC/TiO<sub>2</sub> could not be determined by XRD nor HRTEM, both samples were analyzed by Raman (Figure 4) to identify surface WO<sub>x</sub> species that could be formed when materials were

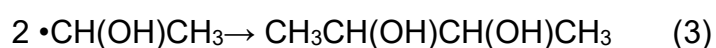
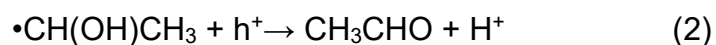
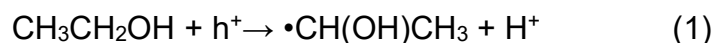
exposed to air [41]. Raman spectrum of WC show bands characteristics of  $\text{WO}_3$ : the bands at 805 and 709  $\text{cm}^{-1}$  correspond to W-O stretching modes, those at 325 and 265  $\text{cm}^{-1}$  to W-O-W bending modes and the bands below 200  $\text{cm}^{-1}$  are assigned to lattice vibrations [42, 43]. According with XRD results, Raman spectrum of  $\text{TiO}_2$ 800 shows bands related with the presence of anatase (bands at 142, 198, 398, 514 and 636  $\text{cm}^{-1}$ ) and rutile (bands at 236, 445 and 610  $\text{cm}^{-1}$ ) [44, 45]. The Raman spectrum of  $\text{WC/TiO}_2$  is very similar to that of  $\text{TiO}_2$ 800, indicating also the only presence of anatase and rutile; for  $\text{WC/TiO}_2$ , bands related with the presence of tungsten oxides were not found. A zoom of the 1200-1700  $\text{cm}^{-1}$  zone in the spectra of WC and  $\text{WC/TiO}_2$  allows to see two low intensity bands with maximum at 1350 and 1600  $\text{cm}^{-1}$  (D and G bands), which can be related with the presence of a low amount of carbonaceous residues. The band-gap values determined from UV-vis DRS and using the Kubelka-Munk formalism (Figure S1) for  $\text{WC/TiO}_2$  and  $\text{TiO}_2$ 800 were 2.85 and 2.87 respectively, slightly lower than that expected for pure rutile (3.00 eV) [46, 47].

WC and  $\text{WC/TiO}_2$  were analyzed by XPS; W 4f, W 4d, C1s, N 1s, Ti 2p and O 1s core level spectra were registered. For WC, the analysis of W 4f spectrum pointed out the presence of surface WC (W 4f<sub>7/2</sub> = 32.6 eV) and  $\text{WO}_3$  (W 4f<sub>7/2</sub> = 36.6 eV) (Figure S2) [47, 48], according with XRD and Raman results. Although the intensity of W 4d is lower than that of W 4f, for  $\text{WC/TiO}_2$ , the W 4d (Figure 5) core level spectrum was analyzed because the overlapping of W 4f and Ti 3p levels. The W 4d peaks were deconvoluted into three doublets W 4d<sub>5/2</sub>:W 4d<sub>3/2</sub>, keeping an intensity ratio W 4d<sub>5/2</sub>:W 4d<sub>3/2</sub>=3:2 and a spin-orbital splitting of 13 eV [49]. The W 4d<sub>5/2</sub> component at 244.2 eV can be reasonably assigned to the presence of surface tungsten carbide [48] and those at higher BE to different tungsten oxide

species (Figure 5A) [48, 50]. Figure 5A also displays the C 1s core level spectrum of WC/TiO<sub>2</sub>, which shows a maximum at 284.8 eV, the component at 283.4 eV is associated to surface tungsten carbide species and those above 284.8 eV to different surface oxygen containing species [51, 52]. Peaks corresponding to N 1s core level were not found (Figure S2), indicating the absence of nitrogen-containing residues coming from the urea used in the preparation. From Ti 2p and O 1s spectra, Ti 2p<sub>3/2</sub> BE of 458.7 eV and O 1s BE of 530.0 eV were found (Figure S2), which corresponded well to those expected for TiO<sub>2</sub>.

For proving the influence of tungsten carbide nanoparticles in the photocatalytic transformation of ethanol<sub>(aq)</sub> (25% v/v) solutions onto TiO<sub>2</sub>, commercial TiO<sub>2</sub> P25, TiO<sub>2</sub>800 and WC/TiO<sub>2</sub> were tested. In all cases, H<sub>2</sub> was the main product obtained; O<sub>2</sub> was not detected in any case. Figure 6 shows that the amount of H<sub>2</sub> produced and the rate of production along 4 hours of catalytic test is higher for WC/TiO<sub>2</sub> than for TiO<sub>2</sub>800 or commercial TiO<sub>2</sub> P25. A clear improvement in the H<sub>2</sub> production is observed when WC nanoparticles are dispersed onto TiO<sub>2</sub> surface, indicating the role of WC as co-catalyst in this system. Besides H<sub>2</sub>, carbon-containing products such CO, CO<sub>2</sub>, CH<sub>4</sub>, C<sub>2</sub>H<sub>4</sub>, C<sub>2</sub>H<sub>6</sub> and acetaldehyde were also found in the gas phase. However, the amount of CO, CO<sub>2</sub>, CH<sub>4</sub>, C<sub>2</sub>H<sub>4</sub> and C<sub>2</sub>H<sub>6</sub> was much lower than that of H<sub>2</sub> (Table 2). As described in the experimental section, the liquid products were analyzed at the end of the catalytic test; acetaldehyde, acetone, 2,3-butanediol and a minor amount of acetal were found (Table 2). As stated above, the use of ethanol aqueous solutions brings the opportunity of producing simultaneously H<sub>2</sub> and valorized compounds coming from ethanol [11]. A first step of the photocatalytic transformation of ethanol<sub>(aq)</sub> over Pt/TiO<sub>2</sub> has been demonstrated to be acetaldehyde or 2,3-butanediol

formation [10, 11]. The reaction of ethanol with the hole on the surface of TiO<sub>2</sub> and the formation of  $\alpha$ -hydroxyethyl radicals ( $\bullet\text{CH}(\text{OH})\text{CH}_3$ ) (eq. 1) has been proposed to be the first step for the acetaldehyde (eq. 2) and 2,3-butanediol formation (eq. 3):



Then, the photogenerated  $\text{e}^-$ , could react with  $\text{H}^+$  on the surface of Pt and  $\text{H}_2$  would be formed. Similar reaction pathways can be reasonably proposed taking place when WC/TiO<sub>2</sub> is used. The small amounts of CO and methane found could be accounted for acetaldehyde decomposition. The addition of ethanol to acetaldehyde could be the responsible of acetal formation. Data in Table 2, indicate that using WC/TiO<sub>2</sub>, a higher amount of acetone and a lower amount of 2,3-butanediol is formed than when TiO<sub>2</sub>800 is used. The photocatalytic transformation of aqueous 2,3-butanediol or acetaldehyde solutions has been demonstrated that produces acetone when Pt/TiO<sub>2</sub> is used [10], these processes could be favored when WC<sub>x</sub> nanoparticles are dispersed onto TiO<sub>2</sub> (Table 2). The used catalyst was characterized after the photocatalytic test by XPS (Figure 5B). The presence of W 4d<sub>5/2</sub> component at 244.1 eV and C 1s at 283.3 eV indicates that tungsten carbide species remained on surface after the photocatalytic test. The new component of C 1s XP spectrum of used-catalyst at about 292 eV can be related to carbonate species [49].

In order to study the durability of WC/TiO<sub>2</sub>, the used catalyst was separated by filtration and a new photocatalytic test was carried out (Figure 7). The used

catalyst showed a slightly lower H<sub>2</sub> production than the fresh one, 5696 mmolg<sup>-1</sup> vs. 6121 mmolg<sup>-1</sup> during 4 h of photocatalytic test.

## **Conclusions**

A WC/TiO<sub>2</sub> photocatalyst containing well-dispersed tungsten carbide (2-3 nm NPs) onto TiO<sub>2</sub> was prepared using a method based on a sol-gel procedure appropriate for the preparation of bulk WC. Different tungsten carbide phases such as hexagonal WC and W<sub>2</sub>C and cubic WC<sub>1-x</sub> were identified in WC/TiO<sub>2</sub>. The photocatalytic behavior for H<sub>2</sub> production from ethanol<sub>aq</sub> of WC/TiO<sub>2</sub> was compared with that of WC-free TiO<sub>2</sub>800 and commercial TiO<sub>2</sub> P25 as reference. WC<sub>x</sub> NPs act as co-catalyst in the process; using WC/TiO<sub>2</sub>, the amount of H<sub>2</sub> yielded during the photocatalytic test was more than a 40 % higher than when TiO<sub>2</sub>800 or TiO<sub>2</sub>(P25) were used. Besides H<sub>2</sub>, acetaldehyde and 2,3-butanediol were obtained from primary ethanol oxidation; then acetone was produced, its formation likely favored by the presence of tungsten carbide NPs. Tungsten carbide species remained on surface of WC/TiO<sub>2</sub> after the photocatalytic test; the amount of H<sub>2</sub> produced with the reused WC/TiO<sub>2</sub> was kept above 93 % of that provided when the fresh sample was used.

## **Acknowledgements**

The authors thank MAT2017-87500-P project for financial support. A. P. thanks MINECO for his PhD grant (BES-C-2015-074574).

## References

- [1] Li D, Li X, Gong J. Catalytic reforming of oxygenates: state of the art and future prospects. *Chem Rev* 2016;116:11529-53. <https://doi.org/10.1021/acs.chemrev.6b00099>
- [2] Mattos LV, Jacobs G, Davis BH, Noronha FB. Production of hydrogen from ethanol: review of reaction mechanism and catalyst deactivation. *Chem Rev* 2012;112:4094-123. <https://doi.org/10.1021/cr2000114>
- [3] Ramírez de la Piscina P, Homs N. Use of biofuels to produce hydrogen (reformation processes), *Chem Soc Rev* 2008;37:2459-67. <https://doi.org/10.1039/B712181B>
- [4] EU Biofuels annual 2019, USDA Foreign Agricultural Service, Gain Report number:NL1902. <https://apps.fas.usda.gov/newgainapi/api/report/downloadreportbyfilename?filename=Biofuels%20Annual%20The%20Hague%20EU-28%208-9%202019.pdf>
- [5] Fajrina N, Tahir M. A critical review in strategies to improve photocatalytic water splitting towards hydrogen production. *Int J Hydrog Energy* 2019;44:540-77. <https://doi.org/10.1016/j.ijhydene.2018.10.200>
- [6] Fontelles-Carceller O, Muñoz-Batista MJ, Conesa JC, Kubacka A, Fernández-García M. H<sub>2</sub> photo-production from methanol, ethanol and 2-propanol: Pt-(Nb)TiO<sub>2</sub> performance under UV and visible light. *Mol Catal* 2018;446:88-97. <https://doi.org/10.1016/j.mcat.2017.12.023>
- [7] Cargnello M, Gasparotto A, Gombac V, Montini T, Barreca D, Fornasiero P. Photocatalytic H<sub>2</sub> and Added-value by-products – The role of metal oxide systems in their synthesis from oxygenates. *Eur J Inorg Chem* 2011;28:4309-23. <https://doi.org/10.1002/ejic.201100532>

- [8] Kondarides DI, Patsoura A, Verykios XE. Anaerobic photocatalytic oxidation of carbohydrates in aqueous Pt/TiO<sub>2</sub> suspensions with simultaneous production of hydrogen. *J Adv Oxid Technol* 2010;13:116-23. <https://doi.org/10.1515/jaots-2010-0115>
- [9] Chen X, Shen S, Guo L, Mao SS. Semiconductor-based photocatalytic hydrogen generation. *Chem Rev* 2010;110:6503-70. <https://doi.org/10.1021/cr1001645>
- [10] Sola AC, Homs N, Ramírez de la Piscina P. Photocatalytic H<sub>2</sub> production from ethanol<sub>(aq)</sub> solutions: The effect of intermediate products. *Int J Hydrogen Energy* 2016;41:19629-36. <https://doi.org/10.1016/j.ijhydene.2016.05.268>
- [11] Sola AC, Ramírez de la Piscina P, Homs N. Behaviour of Pt/TiO<sub>2</sub> catalysts with different morphological and structural characteristics in the photocatalytic conversion of ethanol aqueous solutions. *Catal Today* 2020;341:13-20. <https://doi.org/10.1016/j.cattod.2018.06.017>
- [12] Nomikos GN, Panagiotopoulou P, Kondarides D, Verykios XE. Kinetic and mechanistic study of the photocatalytic reforming of methanol over Pt/TiO<sub>2</sub> catalyst. *Appl Catal B Environ* 2014;146:249-57. <https://doi.org/10.1016/j.apcatb.2013.03.018>
- [13] Kandiel TA, Ivanova I, Bahnemann DW. Long-term investigation of the photocatalytic hydrogen production on platinized TiO<sub>2</sub>: an isotopic study. *Energy Environ Sci* 2014;7:1420-5. <https://doi.org/10.1039/c3ee41511b>
- [14] Sola AC, Homs N, Ramirez de la Piscina P. An in-situ DRIFTS-MS study of the photocatalytic H<sub>2</sub> production from ethanol<sub>(aq)</sub> vapour over Pt/TiO<sub>2</sub> and Pt-Ga/TiO<sub>2</sub> catalysts. *Int J Hydrogen Energy* 2018;43:16922-28. <https://doi.org/10.1016/j.ijhydene.2018.02.098>

- [15] Wong TJ, Lim FJ, Gao M, Lee GH, Ho GW. Photocatalytic H<sub>2</sub> production of composite one-dimensional TiO<sub>2</sub> nanostructures of different morphological structures and crystal phases with graphene. *Catal. Sci Technol* 2013;3:1086-93. <https://doi.org/10.1039/C2CY20740K>.
- [16] Ran J, Zhang J, Yu J, Jaroniec M, Qiao SZ. Earth-abundant cocatalysts for semiconductor-based photocatalytic water splitting *Chem Soc Rev* 2014;43:7787-812. <https://doi.org/10.1039/C3CS60425J>
- [17] Levy RB, Boudart M. Platinum-Like behavior of tungsten carbide in surface catalysis. *Science* 1973;181:547-9. <https://doi.org/10.1126/science.181.4099.547>
- [18] Oyama ST. Introduction to the chemistry of transition metal carbides and nitrides. In: Oyama ST, editors. *The Chemistry of Transition Metal Carbides and Nitrides*, Dordrecht: Springer; 1996, p. 1-27. [https://doi.org/10.1007/978-94-009-1565-7\\_1](https://doi.org/10.1007/978-94-009-1565-7_1)
- [19] Hwu HH, Chen JG. Surface chemistry of transition metal carbides. *Chem Rev* 2005;105:185-212. <https://doi.org/10.1021/cr0204606>
- [20] Guo H, Qi Z, Liu Y, Xia H, Li L, Huan Q, Wang A, Li C. Tungsten-based catalysts for lignin depolymerization: the role of tungsten species in C-O bond cleavage. *Catal Sci Technol* 2019;9:2144-51. <https://doi.org/10.1039/C9CY00251K>
- [21] Bennett LH, Cuthill JR, McAlister AJ, Erickson NE, Watson RE. Electronic structure and catalytic behavior of tungsten carbide. *Science* 1974;184:563-5. <https://doi.org/10.1126/science.184.4136.563>
- [22] Peppernick SJ, Gunaratne KDD, Castleman AW, Superatom spectroscopy and the electronic state correlation between elements and isoelectronic



molecular counterparts 2009;107:975-80.

<https://doi.org/10.1073/pnas.0911240107>

[23] Harnisch F, Sievers G, Schröder U. Tungsten carbide as electrocatalyst for the hydrogen evolution reaction in pH neutral electrolyte solutions. *Appl Catal B Environ* 2009;89:455-58. <https://doi.org/10.1016/j.apcatb.2009.01.003>

[24] Liu Y, Mustain WE. Evaluation of tungsten carbide as the electrocatalyst support for platinum hydrogen evolution/oxidation catalysts. *Int J Hydrogen Energy* 2012;37:8929-38. <https://doi.org/10.1016/j.ijhydene.2012.03.044>

[25] Meyer S, Nikiforov AV, Petrushina IM, Köhler K, Christensen E, Jensen JO, Bjerrum NJ. Transition metal carbides (WC, Mo<sub>2</sub>C, TaC, NbC) as potential electrocatalysts for the hydrogen evolution reaction (HER) at medium temperatures. *Int J Hydrogen Energy* 2015;40:2905-11. <https://doi.org/10.1016/j.ijhydene.2014.12.076>

[26] Hunt ST, Milina M, Wang Z, Leshkov YR. Activating earth-abundant electrocatalysts for efficient, low-cost hydrogen evolution/oxidation: sub-monolayer platinum coatings on titanium tungsten carbide nanoparticles. *Energy Environ Sci* 2016;9:3290-301. <https://doi.org/10.1039/C6EE01929C>

[27] Liu C, Zhou D, Zhou J, Xie Z, Xia Y. Synthesis and characterization of tungsten carbide and application to electrocatalytic hydrogen evolution. *RSC Adv* 2016;6:76307-11. <https://doi.org/10.1039/C6ra12545J>

[28] Ko YJ, Cho JM, Kim I, Jeong DS, Lee KS, Park JK, Baik YJ, Choi HJ, Lee WS. Tungsten carbide nanowalls as electrocatalyst for hydrogen evolution reaction: New approach to durability issue. *Appl Catal B Environ* 2017;203:684-91. <https://doi.org/10.1016/j.apcatb.2016.10.085>

- [29] Wang SL, Zhu Y, Luo X, Huang Y, Chai J, Wong TI, Xu GQ. 2D WC/WO<sub>3</sub> Heterogeneous hybrid for photocatalytic decomposition of organic compounds with VIS-NIR Light. *Adv Funct Mater* 2018;28:1705357-64. <https://doi.org/10.1002/adfm.201705357>
- [30] Garcia-Esparza AT, Cha D, Ou Y, Kubota J, Domen K, Takahabe K. Tungsten carbide nanoparticles as efficient cocatalysts for photocatalytic overall water splitting. *ChemSusChem* 2013;6:168-81. <https://doi.org/10.1002/cssc.201200780>
- [31] Han N, Yang KR, Lu Z, Li Y, Xu W, Gao T, Cai Z, Zhang Y, Batista VS, Liu W, Sun X. Nitrogen-doped tungsten carbide monoarray as an efficient bifunctional electrocatalyst for water splitting in acid. *Nat Commun* 2018;9:24:1-9. <https://doi.org/10.1038/s41467-018-03429-z>
- [32] Shao M, Chen W, Ding S, Lo KH, Zhong X, Yao L, Ip WF, Xu B, Wang X, Pan H. WX<sub>y</sub>/g-C<sub>3</sub>N<sub>4</sub> (WX<sub>y</sub>=W<sub>2</sub>C, WS<sub>2</sub>, or W<sub>2</sub>N) composites for highly efficient photocatalytic water Splitting. *ChemSusChem* 2019;12:3355-62. <https://doi.org/10.1002/cssc.201900844>
- [33] Pan YX, Zhuang HQ, Ma H, Cheng J, Song J. Tungsten carbide hollow spheres flexible for charge separation and transfer for enhanced visible-light-driven photocatalysis. *Chem Eng Sci* 2019;71-7. <https://doi.org/10.1016/j.ces.2018.01.022>
- [34] He K, Xie J, Yang Z, Shen R, Fang Y, Ma S, Chen X, Li X. Earth-abundant WC nanoparticles as an active noble-metal-free-co-catalyst for the highly boosted photocatalytic H<sub>2</sub> production over g-C<sub>3</sub>N<sub>4</sub> nanosheets under visible light. *Catal Sci Technol* 2017;11:193-202. <https://doi.org/10.1039/C7CY00029D>

- [35] Jang JS, Ham DJ, Lakshminarasimhan N, Choi WY, Lee JS. Role of platinum-like tungsten carbide as cocatalysts of CdS photocatalyst for hydrogen production under visible light irradiation. *Appl Catal A Gen* 2008;346:149-54. <https://doi.org/10.1016/j.apcata.2008.05.020>
- [36] Oosawa Y. Photocatalytic hydrogen evolution from an aqueous methanol solution over ceramics-electrocatalyst/TiO<sub>2</sub>. *Chem Lett* 1983;12:577-80. <https://doi.org/10.1246/cl.1983.577>
- [37] Giordano C, Erpen C, Yao W, Antonietti M. Synthesis of Mo and W carbide and nitride nanoparticles via a simple 'urea glass' route. *Nano Lett* 2008;8:4659-63. <https://pubs.acs.org/doi/10.1021/nl8018593>
- [38] Jackman MJ, Thomas AG, Muryn C. Photoelectron spectroscopy study of stoichiometric and reduced anatase TiO<sub>2</sub>(101) surfaces: The effect of subsurface defects on water adsorption at near-ambient pressures. *J Phys Chem C* 2015;119:13682-90. <https://doi.org/10.1021/acs.jpcc.5b02732>
- [39] Zang H, Banfiels JF. Understanding polymorphic phase transformation behavior during growth of nanocrystalline aggregates: insights from TiO<sub>2</sub>. *J Phys Chem B* 2000;3481-7. <https://doi.org/10.1021/jp000499j>
- [40] Reyes-Coronado D, Rodriguez-Gattorno G, Espinosa-Pesqueira ME, Cab C, De Coss R, Oskam G. Phase-pure TiO<sub>2</sub> nanoparticles: anatase, brookite and rutile. *Nanotechnology* 2008;145605-14. <https://doi.org/10.1088/0957-4484/19/14/145605>
- [41] Mamede AS, Payen E, Grange P, Poncelet G, Ion A, Alifanti M, Pârvulescu VI. Characterization of WO<sub>x</sub>/CeO<sub>2</sub> catalysts and their reactivity in the isomerization of hexane. *J Catal* 2004;223:1-12. <https://doi.org/10.1016/j.jcat.2004.01.008>

- [42] Santato C, Odziemkowski M, Ulman M, Augustynski J. Crystallographically oriented mesoporous WO<sub>3</sub> films: synthesis, characterization and applications. *J Am Chem Soc* 2001;123:10639-49. <https://doi.org/10.1021/ja011315x>
- [43] Takase A, Miyakawa K. Raman study on sol-gel derived tungsten oxides from tungsten ethoxide. *Jpn J Appl Phys* 1991;1508-11. <https://doi.org/10.1143/JJAP.30.L1508>
- [44] Zhang J, Li M, Feng Z, Chen J, Li C. UV Raman spectroscopic study on TiO<sub>2</sub>. I. Phase transformation at the surface and in the bulk. *J Phys Chem B* 2006;110:927-35. <https://doi.org/10.1021/jp0552473>
- [45] Kelly S, Pollak FH, Tomkiewicz M. Raman spectroscopy as a morphological probe for TiO<sub>2</sub> aerogels. *J Phys Chem B* 1997;101:2730-4. <https://doi.org/10.1021/jp962747a>
- [46] Leung DY, Fu X, Wang C, Ni M, Leung MKH, Wang X, Fu X. Hydrogen production over titania-based photocatalysts. *ChemSusChem* 2010;3:681-94. <https://doi.org/10.1002/cssc.201000014>
- [47] Shimura K, Yoshida H. Heterogeneous photocatalytic hydrogen production from water and biomass derivatives. *Energy Environ Sci* 2011;4:2467-81. <https://doi.org/10.1039/C1EE01120K>
- [48] McGuire GE, Schweitzer GK, Carlson TA. Study of core electron binding energies in some group IIIa, Vb and VIb compounds. *Inorg Chem* 1973;12:2450-3. <https://doi.org/10.1021/ic50128a045>
- [49] Moulder JF, Stickle WF, Sobol PE, Bomben KD. *Handbook of X-ray Photoelectron Spectroscopy*. Minnesota: Perkin-Elmer Corporation; 1992.
- [50] Xie FY, Gong L, Liu X, Tao YT, Zhang WH, Chen SH, Meng H, Chen J. XPS studies on surface reduction of tungsten oxide nanowire film by Ar<sup>+</sup>

bombardment. J Electron Spectrosc Relat Phenom 2012;185:112-8.

<https://doi.org/10.1016/j.elspec.2012.01.004>

[51] Leclercq G, Kamal M, Giraudon JM, Devassine P, Feigenbaum L, Leclercq L, Frennet A, Bastin JM, Lofberg A, Decker S, Dufour M. Study of the preparation of bulk powder tungsten carbides by temperature programmed reaction with CH<sub>4</sub>+H<sub>2</sub> mixtures. J Catal 1996;142-69. <https://doi.org/10.1006/jcat.1996.0015>

[52] Krasovskii PV, Malinovskaya OS, Samokhin AV. XPS study of Surface chemistry of tungsten carbides nanopowders produced through DC thermal plasma/hydrogen annealing process. Appl Surf Sci 2015;339:46-54. <https://doi.org/10.1016/j.apsusc.2015.02.152>

## Legends to the Figures

**Figure 1.** XRD patterns of bulk WC, TiO<sub>2</sub>800 and WC/TiO<sub>2</sub>.

**Figure 2.** SEM image and EDX mapping of WC/TiO<sub>2</sub>. On the bottom a representative EDX analysis.

**Figure 3.** TEM (A and B) and HRTEM (C and D) images of WC/TiO<sub>2</sub> sample. Particle size distribution (inset in C).

**Figure 4.** Raman spectra of WC, TiO<sub>2</sub>800 and WC/TiO<sub>2</sub>. On the right part zoom of the 1225-1625 cm<sup>-1</sup> zone.

**Figure 5.** XP spectra of W 4d and C 1s core levels corresponding to WC/TiO<sub>2</sub>: A) fresh catalyst; B) after the photocatalytic test.

**Figure 6.** Amount of H<sub>2</sub> produced and H<sub>2</sub> production rate (inset) along irradiation time for WC/TiO<sub>2</sub>, TiO<sub>2</sub>800 and TiO<sub>2</sub>(P25) during the photocatalytic transformation of ethanol<sub>aq</sub> solution (25% v/v) at 298 K. 500 mg of catalysts were used in all cases.

**Figure 7.** Reusability of WC/TiO<sub>2</sub> catalyst. Comparison of H<sub>2</sub> produced along irradiation time for fresh and reused WC/TiO<sub>2</sub> during the photocatalytic transformation of ethanol<sub>aq</sub> solution (25% v/v) at 298 K. 170 mg of catalysts were used in both cases.